Protein Storage Vacuoles Are Transformed into Lytic Vacuoles in Root Meristematic Cells of Germinating Seedlings by Multiple, Cell Type-Specific Mechanisms[1][W]

Huiqiong Zheng* and L. Andrew Staehelin

Institute of Plant Physiology and Ecology, Shanghai Institutes for Biological Sciences, Chinese Academy of Sciences, Shanghai 200032, China (H.Z.); and Department of Molecular and Cellular Biology, University of Colorado, Boulder, Colorado 80309 (L.A.S.)

We have investigated the structural events associated with vacuole biogenesis in root tip cells of tobacco (*Nicotiana tabacum*) seedlings preserved by high-pressure freezing and freeze-substitution techniques. Our micrographs demonstrate that the lytic vacuoles (LVs) of root tip cells are derived from protein storage vacuoles (PSVs) by cell type-specific sets of transformation events. Analysis of the vacuole transformation pathways has been aided by the phytin-dependent black osmium staining of PSV luminal contents. In epidermal and outer cortex cells, the central LVs are formed by a process involving PSV fusion, storage protein degradation, and the gradual replacement of the PSV marker protein α-tonoplast intrinsic protein (TIP) with the LV marker protein γ-TIP. In contrast, in the inner cortex and vascular cylinder cells, the transformation events are more complex. During mobilization of the stored molecules, the PSV membranes collapse osmotically upon themselves, thereby squeezing the vacuolar contents into the remaining bulging vacuolar regions. The collapsed PSV membranes then differentiate into two domains: (1) vacuole "reinflation" domains that produce pre-LVs, and (2) multilamellar autophagosomal domains that are later engulfed by the pre-LVs. The multilamellar autophagosomal domains appear to originate from concentric sheets of PSV membranes that create compartments within which the cytoplasm begins to break down. Engulfment of the multilamellar autophagic vacuoles by the pre-LVs gives rise to the mature LVs. During pre-LV formation, the PSV marker α-TIP disappears and is replaced by the LV marker γ-TIP. These findings demonstrate that the central LVs of root cells arise from PSVs via cell type-specific transformation pathways.

Despite their structural simplicity, vacuoles remain one of the least well-understood organelles of plant cells. Not only do plant cells contain different types of vacuoles that serve a multitude of functions (Wink, 1993; De, 2000; Frigerio et al., 2008; Xu et al., 2010), but the architecture of a given vacuole system can change dramatically both during the cell cycle (Seguí-Simarro and Staehelin, 2006) and development (Oda et al., 2009). In addition, the question of whether all vacuoles are derived from existing vacuoles or if some can be created de novo has yet to be answered in an unambiguous manner (Robinson and Hinz, 1997; Marty, 1999; Oda et al., 2009; Zouhar and Rojo, 2009).

The two main types of vacuoles of plant cells are the lytic vacuoles (LVs) and the protein storage vacuoles (PSVs; De, 2000). The seeds of higher plants accumulate large amounts of storage proteins during seed development and maturation. Those proteins are typically stored in PSVs, which serve as intermediate storage compartments for nitrogen and carbon reserves and minerals, all of which are needed for early seedling growth (Herman and Larkins, 1999; Wang et al., 2007). Mobilization of stored compounds in germinating seeds does not occur in all cells and tissues simultaneously but follows specific spatial and temporal patterns (Hara and Matsubara, 1980; Bethke et al., 1998; Tiedemann et al., 2000). These changes have been documented by following globulin mobilization using both histological stains and immunohistochemical analyses (Höglund et al., 1992; Tiedemann et al., 2000). For example, in vetch (*Vicia sativa*), the first storage proteins to be mobilized, 2 to 3 d post germination, are those located in embryo axis cells; mobilization of the globulins stored in the cotyledons typically starts thereafter (Schlereth et al., 2000; Tiedemann et al., 2000). Further studies have shown that the sites of mobilization of the protein reserves coincide with the sites of growth and differentiation in the embryonic axes, such as in the radicles, where globulin breakdown starts in the epidermis and prevascular strands and then proceeds toward the embryonic shoot. Most likely, this sequence of events is designed to allow for the development of the vascular system before the amino acids are mobilized in the cotyledons and sent to the embryo axis cells (Tiedemann et al., 2001). During

[1] This work was supported by the National Institutes of Health (grant no. GM–61306 to L.A.S.) and the National Basic Research Program of China (grant no. 2011CB710902).

* Corresponding author; e-mail hqzheng@sippe.ac.cn.

The author responsible for distribution of materials integral to the findings presented in this article in accordance with the policy described in the Instructions for Authors (www.plantphysiol.org) is: Huiqiong Zheng (hqzheng@sippe.ac.cn).

[W] The online version of this article contains Web-only data.
www.plantphysiol.org/cgi/doi/10.1104/pp.110.170159

mobilization of the reserves, the PSVs become more acidic and acquire hydrolytic enzymes, and these physiological changes are accompanied by major changes in PSV structure (Ashton, 1976; Van der Wilden et al., 1980; Bethke et al., 1998; Tiedemann et al., 2000, 2001; Jiang et al., 2001, Saito et al., 2002; He et al., 2007; Wang et al., 2007).

Over the past 40 years, a multitude of structural and immunocytochemical studies have focused on the biogenesis of plant vacuoles (Robinson and Hinz, 1997; Bethke et al., 1998; Marty, 1999; Frigerio et al., 2008; Oda et al., 2009; Zouhar and Rojo, 2009). However, a unified hypothesis of how the central LVs of vegetative plant cells are formed has yet to be developed. According to Marty (1978, 1999), the LVs of meristematic cells in root tips are formed by a system of autophagic, provacuolar tubules that originate from trans-Golgi membranes and stain with zinc-iodide osmium. An alternative hypothesis (Amelunxen and Heinze, 1984; Hilling and Amelunxen, 1985) suggests that LVs arise from smooth endoplasmic reticulum (ER) tubules, which line up in a spherical configuration roughly equivalent in size to the future central vacuole and then fuse laterally to produce the new vacuolar membrane. In aleurone cells, the process of LV formation appears to involve coalescence of the PSVs, acidification of the vacuole lumen, and mobilization of the stored molecules (Bethke et al., 1998). The multivacuole concept of Paris et al. (1996) postulates that young root tip cells contain two separate types of vacuoles, PSVs and LVs, which fuse with each other to form the large central vacuole. This hypothesis has been challenged by Olbrich et al. (2007) and by Hunter et al. (2007), whose PSV and LV marker protein studies have demonstrated that root cells contain only one type of vacuole.

We have employed a combination of high-pressure freezing and freeze-substitution methods to preserve the three-dimensional architecture of the vacuolar membranes of tobacco (*Nicotiana tabacum*) root tip cells during imbibition, germination, and early development to determine if the LVs are created de novo or if they develop from existing vacuoles. Our micrographs demonstrate that the central LVs of vegetative root cells arise from PSVs after the storage molecules of the latter have been mobilized. The actual PSV-to-LV transformation process involves cell type-specific changes in vacuole architecture, the formation of distinct, transient membrane configurations, and the replacement of α-tonoplast intrinsic protein (TIP) with γ-TIP aquaporin channels.

RESULTS

The images presented in this paper are of tobacco seedlings grown 1 to 6 d after sowing (DAS) and preserved for microscopic analysis by high-pressure freezing and freeze-substitution methods (Figs. 1–4 and 6–8; Supplemental Figs. S1–S8). The quality of the samples used for the analysis is evident in the micrographs of the longitudinally sectioned roots illustrated in Figure 1 and Supplemental Figures S1 and S2. In these samples, it is not only easy to identify the different cell types using structural criteria but also to follow the characteristic changes in cell and tissue architecture associated with germination and seedling growth. During the first 24 h of germination, the changes in tissue structure reflect the process of hydration, with little evidence of changes in organelle structure due to metabolic activities (Fig. 1A), even though an occasional dividing cell is seen (data not shown). For this reason, our analysis of vacuole development has focused on the 2- to 6-DAS root samples.

Germinating Roots Contain Four Types of Structurally Distinct PSVs

In longitudinal sections of tobacco seedlings hydrated for 24 h (1 DAS), the radicle is seen to be

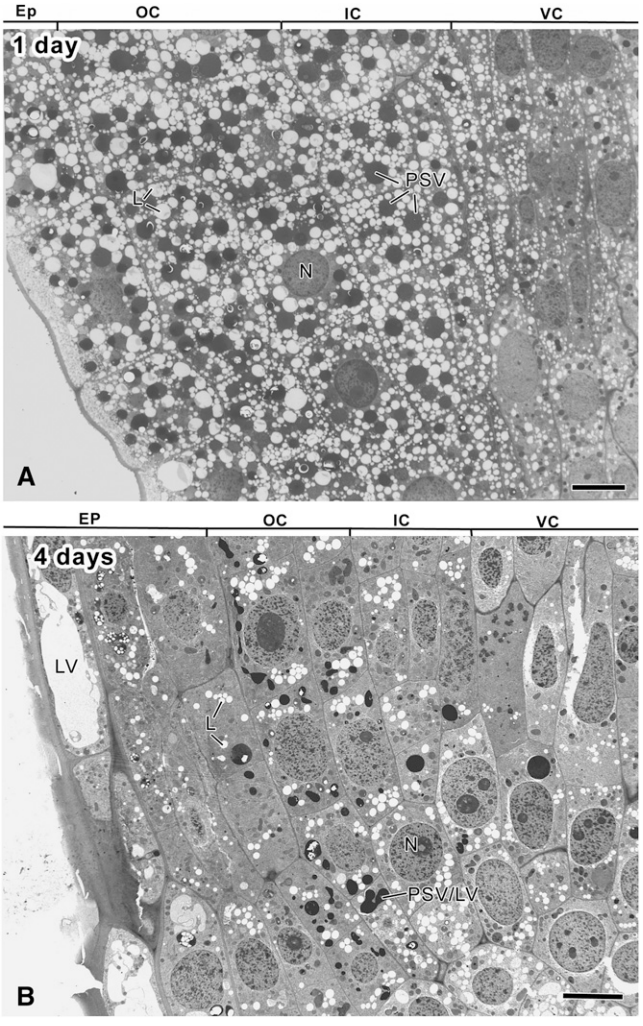

Figure 1. Electron micrographs depicting the organization of the apical meristem of longitudinally sectioned tobacco root tips at 1 (A) and 4 (B) DAS. EP, Epidermis; OC, outer cortex; IC, inner cortex (endodermis); VC, vascular cylinder; L, lipid body; N, nucleus; PSV/LV, transitional-type vacuole. Bars = 10 μm.

composed of four types of tissues: the vascular cylinder, the cortex, the root cap, and the epidermis, with the cells of the latter sharing a common origin with some of the root cap cells (Fig. 1A; Supplemental Fig. S1). Closer inspection of the different meristematic cell types demonstrates that these tissues contain four structurally distinct types of PSVs (Fig. 2). Type I PSVs are seen in epidermal cells, type II PSVs in outer cortex cells, type III PSVs in inner cortex cells, and type IV PSVs in vascular cylinder cells. As shown below, all of these PSVs are transformed into LVs during early seedling development, but the transformation pathways differ for the different types of PSVs.

A defining feature of type I PSVs of epidermal cells in 1-DAS seedlings (Fig. 2A) is the uneven staining of their proteinaceous contents. These type I PSVs also exhibit the fastest rate of storage molecule mobilization, as evidenced by the reduction of stainable vacuolar contents over time (Supplemental Fig. S3, A–D). Typically, dissolution of the globoids and fusion of the PSVs into larger vacuoles is completed within 2 to 3 DAS, and by 3 DAS, the luminal contents of most of these vacuoles stain lightly, their volume is enlarged, and their morphology begins to resemble the morphology of LVs (Supplemental Fig. S3, B and D). By 4 DAS, transformation of the type I PSVs to central LVs is complete, with the newly formed large central vacuole essentially lacking stainable contents (Supplemental Fig. S3E).

The type II PSVs of outer cortex cells contain large globoids embedded in an osmiophilic, proteinaceous matrix (Fig. 2B). The brittle globoids lack a limiting membrane and frequently shatter during microtomy, leaving behind only small fragments of material around the globoid edges. To determine the elemental composition of intact globoids and of the surrounding matrix materials, we have analyzed unstained thin sections by means of energy-dispersive x-ray spectroscopy (EDXS) analysis (Fig. 2, E and F). The principal components of the globoids were potassium, calcium, magnesium, and phosphorus, consistent with the results of other studies in which the phosphorus signal was traced to phytin, a salt of phytic acid (myoinositol-hexakisphosphate), and potassium, calcium, and magnesium (Lott et al., 1995). The presence of a phosphate peak in the matrix surrounding the globoids suggests that it too contains osmium-binding phytic acid and that the strong (black) osmium staining of the luminal contents of the PSVs in root tip cells is most likely due to phytin (Fig. 2, B–D). This type of osmium staining of the vacuolar contents has not only greatly facilitated identification of the transitional PSV/LV-type vacuoles during later stages of root development but has also helped us elucidate mechanistic aspects of the PSV-to-LV transformation process (see below). Some type II PSVs of 1-DAS outer cortex cells also contained crystalloids (up to 0.8 × 1.4 μm in size; Supplemental Fig. S4). Protein degradation in type II PSVs was slow, and the dark osmium staining of some of these vacuoles persisted for up to 4 to 6 DAS (Figs. 1B and 3).

In structural terms, the type III and type IV PSVs of the inner cortex and vascular cylinder cells, respectively, are very similar (Figs. 1B and 2, C and D). Both types lack crystalloids. However, all type III PSVs in inner cortex cells contained small globoids, whereas the type IV PSVs of vascular cylinder cells mostly lacked globoids and were typically smaller than the type III PSVs. Degradation of type III and type IV PSVs produced collapsed vacuolar compartments with characteristic double membrane structures, some of which were subsequently reinflated to form structural

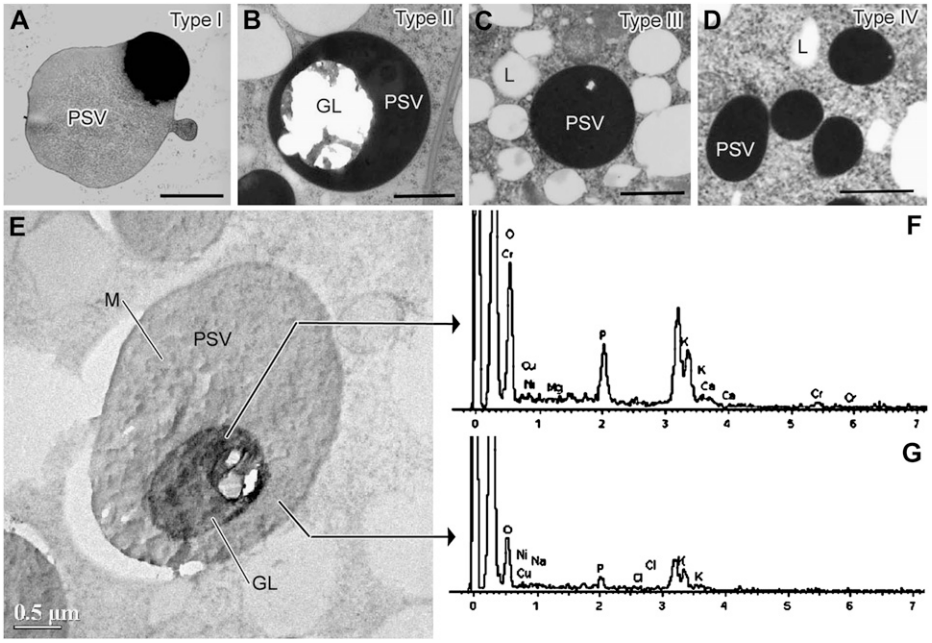

Figure 2. Structure and ionic composition of PSVs in different types of tobacco root tip meristematic cells. A to D, Cell type-specific differences in PSV structure as seen in high-pressure frozen, freeze-substituted, and osmium-stained roots of 1-d-old seedlings. A, Type I PSV in an epidermis cell. B, Type II PSV in an outer cortex cell. C, Type III PSV in an inner cortex (endodermal) cell. D, Type IV PSV in a vascular cylinder cell. E, Detail of a unstained type II PSV. Crystalline globoids (GL) are most prominent in PSVs of outer cortex cells (B and E). Due to the brittle nature of the globoids, they frequently shatter during sectioning, leaving fragments attached to the edges of round holes (B). F and G, The PSV in E was used to produce the EDXS spectrum of a globoid (F) and in the surrounding PSV matrix (G). L, Lipid body; M, PSV matrix. Bars = 1 μm in A to D and 0.5 μm in E.

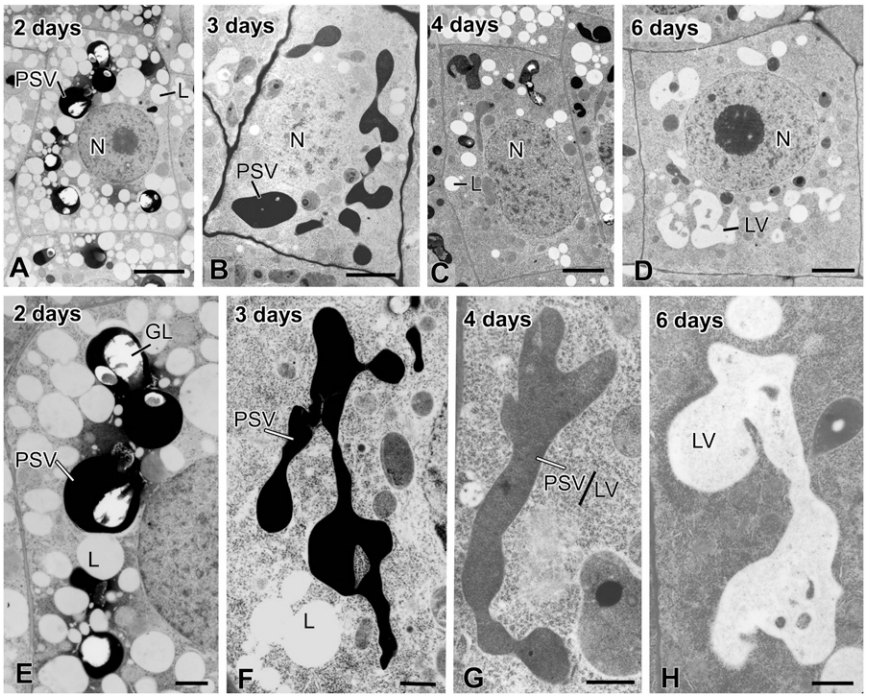

Figure 3. Electron micrographs of outer cortex cells and their vacuoles in tobacco root tips at 2 to 6 DAS. A and E, In 2-d cells, the PSVs, some of which have begun to fuse, are spherical or oval and contain large globoids (GL). B and F, In 3-d cells, the fused PSVs have evolved into large, tubular vacuoles that extend the length of the cells. Solubilization of the globoids is complete, and the uniformly dispersed luminal contents exhibit an intense black staining. C and G, In 4-d cells, the vacuoles (PSV/LV) exhibit a hybrid-type staining pattern, with the luminal contents being less densely stained than in PSVs (see F) but more densely stained than in LVs (see H). The size and shape of the vacuoles are unchanged. D and H, In 6-d cells, the PSV-to-LV transformation is complete, as evidenced by the lack of staining of the luminal contents and by the size of the vacuoles. L, Lipid body; N, nucleus. Bars = 5 μm in A to D and 500 nm in E to H.

membrane domains we have termed pre-LVs, while others became limiting membranes of multilamellar autophagosomes that were subsequently engulfed by the pre-LVs. A detailed description of these developmental changes is presented below.

During Development of the Outer and Inner Cortex and Vascular Cylinder Cells, the Type II, III, and IV PSVs Undergo Characteristic Changes in Architecture as They Metamorphose into LVs

Outer Cortex Cell Development

The first evidence of reserve mobilization in the type II PSVs of outer cortex cells was seen in 2-DAS seedlings (Fig. 3, A and E). In particular, the globoids in the swollen PSVs exhibited fewer signs of shattering, and in many instances their texture became more granular. By 3 DAS, essentially all globoids had disappeared and all of the round PSVs had fused into a characteristic, intensely stained vacuolar network that extended throughout the cytoplasm (Fig. 3, B and F). In parallel, a major reduction in lipid bodies was observed. During the postgerminative period (4–6 DAS), the staining of the vacuolar contents gradually decreased, while only minor changes in vacuolar shape and volume were seen (Fig. 3, C and G), eventually yielding LV-type vacuoles with a very lightly stained lumen (Fig. 3, D and H).

Inner Cortex (Endoderm) Cell Development

The most notable changes in the type III PSVs of inner cortex cells during the first 2 DAS are a general swelling of the spherical vacuoles followed by the fusion of adjacent PSVs with only minor changes in vacuole geometry (Fig. 4, A and E). The increase in PSV volume (approximately 38%) was similar to the overall increase in cell volume (approximately 44%), suggesting that this initial PSV swelling was related to the uptake of water and not due to metabolic activities (Fig. 5; Supplemental Table S1). However, this initial increase in vacuole volume was followed by a huge (approximately 70%) decrease in vacuole volume between 2 and 3 DAS (Fig. 5). Interestingly, the tonoplast surface area only decreased by approximately 30% during the same time period (Fig. 5). The structural basis for this volume change can be seen in Figure 4, B, F, G, and I. In particular, the images suggest that as the vacuolar contents are withdrawn, the tonoplast membranes collapse onto each other (Fig. 4I), squeezing the remaining intensely stained protein/phytin molecules into the bulging domains of the vacuoles. These changes in vacuole architecture resemble the changes in shape of a basketball from which the air has been withdrawn.

Between 3 and 6 DAS, the remaining matrix molecules gradually disappear from the vacuolar lumen, as evidenced by the gradual decrease in staining of the vacuolar contents (Fig. 4, C, D, G, and H). However, during this latter reserve mobilization process, 4 to 6 DAS, the vacuole surface area remains virtually unchanged, while the vacuole volume begins to increase again (Fig. 5). This increase in vacuole volume appears to coincide with the reinflation of some of the collapsed tonoplast membrane domains (Fig. 4, H and J) and the formation of vacuolar structures we have named pre-LVs for the reasons described below. The

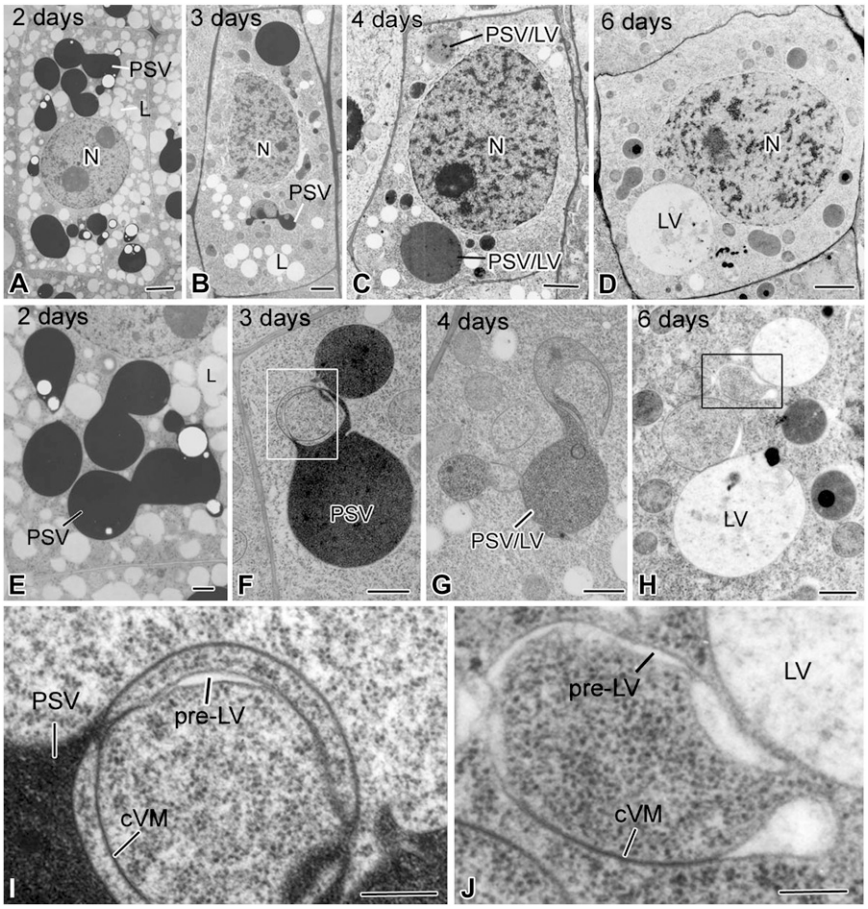

Figure 4. Electron micrographs of meristematic inner cortex (endodermal) cells and of their vacuoles in tobacco root tips at 2 to 6 DAS. A and E, In 2-d cells, the darkly stained PSVs are swollen and have begun to fuse, but the general shape of the individual PSVs is still evident. B and F, In 3-d cells, the PSVs have merged into a few large vacuoles, whose luminal contents exhibit variable staining. Furthermore, their boundary membrane appears continuous with collapsed vacuole membrane (cVM) domains where no luminal contents are seen (I). C and G, In 4-d cells, the vacuoles (PSV/LV) are of a hybrid type based on the lighter staining of their luminal contents. The collapsed membrane domains are more extensive than in the 3-d cells. D and H, In 6-d cells, several types of vacuolar structures are seen: LVs, collapsed vacuole membrane domains, pre-LV domains with translucent luminal contents (J), and autophagic vacuole-type domains (Fig. 7). Boxes in F and H indicate the collapsed vacuole membrane domains shown in I and J. L, Lipid body; N, nucleus. Bars = 2 μm in A to D, 500 nm in E to H, and 200 nm in I and J.

remaining nonswollen, collapsed membrane domains become multilamellar autophagic vacuoles (Fengsrud et al., 2000) that subsequently also contribute to the formation of the large, central LVs.

Vascular Cylinder Cell Development

Figure 6, A and E, illustrate type IV PSVs of vascular cylinder cells in a 2-DAS radicle. All of the PSVs in these cells were densely stained but lacked identifiable, phytin-containing globoids. The images also demonstrate that by 2 DAS, the majority of the PSVs had already fused into multilobed aggregates. Indeed, the first evidence for type IV PSV fusion is detectable in 1-DAS seedlings (data not shown). The subsequent changes in vacuole architecture between 2 and 4 DAS (Fig. 6, A–C and E–G) closely resemble those seen in the inner cortex cells (Fig. 4, A–C and E–G). Most notably, the vacuolar membranes appear to collapse onto each other as the vacuolar matrix molecules are mobilized, and the remaining ones are squeezed into the darkly staining, bulging vacuole domains. By 6 DAS, virtually all of the stainable luminal contents of the bulging vacuolar domains are gone, but many collapsed vacuolar membranes persist throughout the cytoplasm. As described below, as some of these domains begin to reinflate, other domains are used to form what appear to be multilamellar autophagic vacuoles (Fig. 6, D, H, and J).

Reinflation of Collapsed Type III and Type IV PSV Membrane Domains Produces Pre-LVs and Is Accompanied by a Decrease in the PSV Marker α-TIP and an Increase in the LV Marker γ-TIP

Type III and IV PSVs with collapsed tonoplast membranes were observed as early as 3 DAS in inner cortex (Figs. 4, B, F, and I, and 7A) and vascular cylinder cells (Fig. 6, B, F, and I; Supplemental Fig. S5A). These collapsed membrane domains became more extensive during 4 and 5 DAS (Fig. 7, A–D), in parallel with the disappearance of the remaining vacuolar contents (Figs. 4, F–H, and 6, F–H). The end point of this reserve mobilization process appeared to coincide with the disappearance of uniformly stained vacuolar contents and the appearance of stained aggregates of flocculent materials in the remaining swollen vacuole domains (Figs. 4, D and H, and 7, D, E, and H).

The end point of reserve mobilization also appears to coincide with the onset of the actual PSV-to-LV transformation process, as evidenced both by the

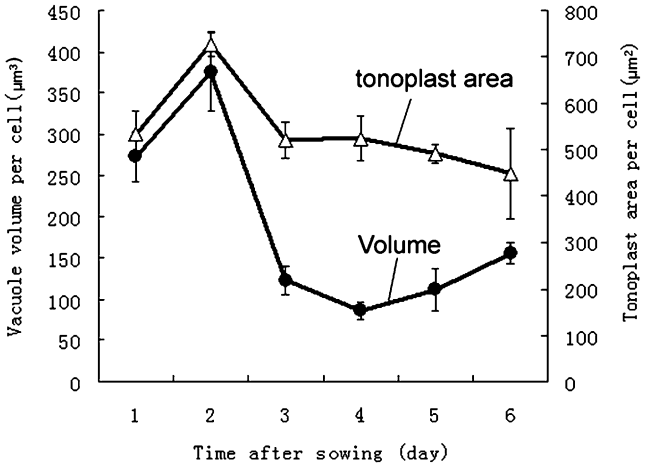

Figure 5. Quantitative changes in volume and tonoplast membrane surface area of PSVs, PSV/LVs, and LVs in inner cortex cells of tobacco root tips at 1 to 6 DAS. Fifty to 150 cells from 10 to 15 different roots per time point were measured. The mean ± SD was calculated for each data point.

changes in vacuole architecture and by the changes in TIP composition of the tonoplast membranes (Figs. 7 and 8). The first changes in vacuole architecture are seen at the interface regions between the remaining bulbous regions of the PSVs and the collapsed tonoplast membrane domains. In particular, in these transitional regions, the collapsed membranes are seen to become physically separated, suggesting that a "vacuole reinflation" process is associated with the formation of the pre-LV domains (Fig. 7; Supplemental Figs. S5 and S7).

To determine if this structural reinflation process reflects an underlying biochemical remodeling of the tonoplast membranes, we have immunolabeled thin sections of 3-, 4-, and 6-DAS high-pressure frozen root samples embedded in LR White resin with anti-α-TIP and anti-γ-TIP antibodies, which are widely used markers for PSV and LV vacuoles, respectively (Jauh et al., 1999). It should be noted that due to the omission of osmium staining of the samples and the use of LR White resin as the embedding medium for the immunolabeling experiments (Fig. 8), the vacuole contents do not become darkly stained and the vacuolar membranes are not as well preserved, as in the Spurr's resin-embedded samples used for the structural analyses (Figs. 3, 4, and 6). Thus, the correlation between vacuole types is based on DAS of the samples and geometry of the vacuoles and not on the staining of the vacuolar contents. As documented in Figure 8, A and B, the tonoplast membranes of the 3-DAS vacuoles label heavily with the anti-α-TIP but not with the anti-γ-TIP antibodies, thus confirming the PSV nature of these vacuoles. In the 4-DAS samples (Fig. 8, C and D), the collapsed tonoplast membranes also label heavily with the anti-α-TIP antibodies. However, coinciding with the appearance of the pre-LV domains, the membranes also show the first evidence of labeling with the

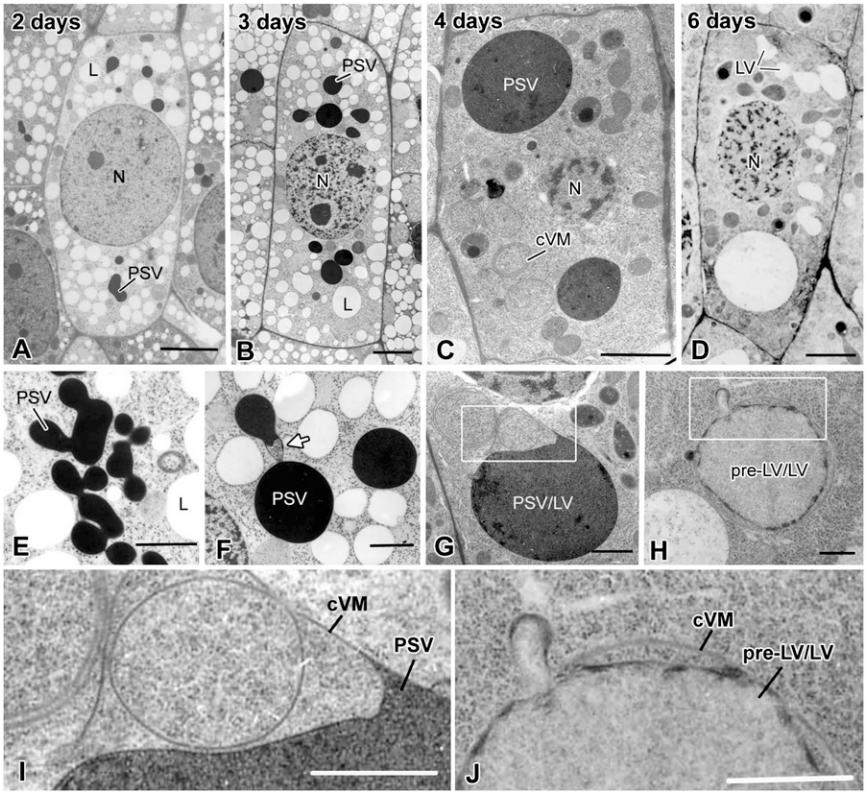

Figure 6. Electron micrographs of meristematic vascular cylinder cells and their vacuoles in tobacco root tips at 2 to 6 DAS. A and E, In 2-d cells, the very darkly stained PSVs lack phytin globoids and appear fused into large, multilobed vacuolar systems. B and F, In 3-d cells, the darkly stained vacuoles are mostly round and their membranes are continuous with collapsed vacuole membrane (cVM) domains (arrow). C and G, The vacuoles in the 4-d cells are of the PSV/LV hybrid type, and their membranes are continuous with very extensive collapsed membrane domains (I). The staining of the vacuolar contents is variable, and occasionally fragments of membrane-like structures are also seen within the vacuoles (Fig. 7E). D and H, In 6-d roots, some cells possess a mixture of mature LVs with unstained lumina, whereas others contain pre-LV/LV/autophagic-type vacuoles with typically lightly stained, flocculent contents and patches of darkly staining material. These vacuoles also show evidence of fusion of small vesicular structures with the large vacuoles (J). More detailed images of hybrid- and autophagic-type vacuoles are presented in Figure 7 and in Supplemental Figure S6. Boxes in G and H indicate the collapsed vacuole membrane domains shown in I and J. N, Nucleus. Bars = 2 μm in A to D, 500 nm in E to H, and 200 nm in I and J.

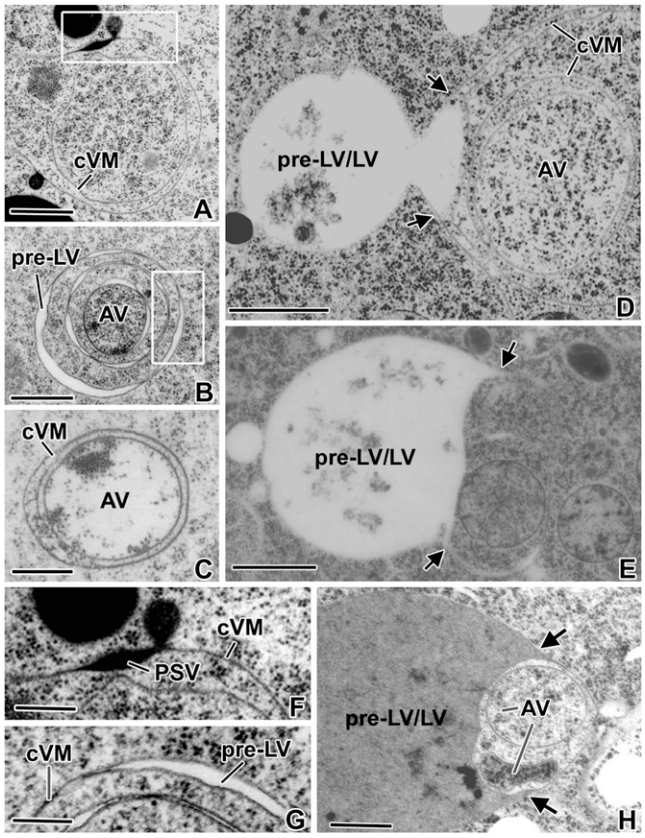

Figure 7. Higher magnification views of collapsed vacuole membranes, pre-LVs, and autophagic vacuoles of inner cortex and vascular bundle cells of 3- to 6-d plants. A and F, Example of the extensive collapsed vacuole membrane (cVM) domains seen in cells where the mobilization of the PSV reserves is nearly complete. The concentric organization of such collapsed vacuole membranes is also seen in D. B and G, Concentric, collapsed vacuole membranes in the process of differentiating into multiple pre-LVs and a central autophagic vacuole (AV) region. C, Autophagic vacuole surrounded by concentric collapsed vacuole membranes. E and H, Advanced-stage pre-LV/LVs in the process of expanding (arrows) into the outermost concentric collapsed vacuole membranes that surround sets of inner concentric collapsed membranes with trapped cytoplasm and autophagic vacuoles. Bars = 0.5 μm in A to C, 1 μm in D, E, and H, and 200 nm in F and G.

anti-γ-TIP antibodies, thereby indicating that the vacuole transformation process had begun by this stage of vacuole development. By 6 DAS, the density of the membrane-associated anti-γ-TIP antibody labeling was substantial (Fig. 8F; Supplemental Fig. S9C shows an image of the entire LV depicted in Figure 8F, whose membrane is labeled with more than 20 gold particles). In contrast, no membrane labeling was seen with the anti-α-TIP antibodies in the 6-DAS cells (Fig. 8E; Supplemental Fig. S9A). Interestingly, all of the residual anti-α-TIP labeling of the 6-DAS samples was seen to be associated with flocculent material in the lumen of the nascent LVs (Fig. 8E), suggesting internalization of the no longer needed PSV-type membrane molecules.

In Inner Cortex and Vascular Cylinder Cells, Subdomains of the Collapsed PSV Membranes Give Rise to Multilamellar Autophagosomes That Are Subsequently Engulfed by Adjacent Pre-LVs

Both the extent to which autophagic vacuole formation contributes to LV formation and the type of membrane systems involved in autophagosome formation are not well understood (Hoh et al., 1995; Robinson and Hinz, 1997; Marty, 1999; Bassham, 2009). In 4- to 6-DAS roots, the collapsed tonoplast membranes in inner cortex and vascular cylinder cells frequently formed concentric membrane rings that enclosed significant volumes of cytoplasm (Figs. 7, A–D, and 8C; Supplemental Fig. S5, A and B). Within

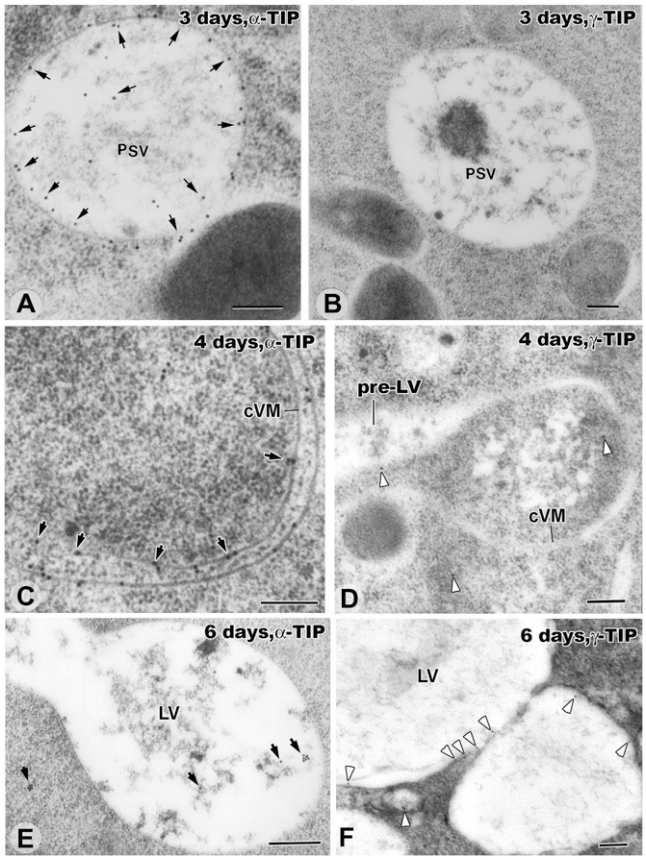

Figure 8. Immunogold localization of α-TIP and γ-TIP in the tonoplast membranes of inner cortex cells in 3-, 4-, and 6-d seedlings. Note that, unlike in Figures 1, 4, 6, and 7, the samples have not been stained with osmium and that, for this reason, the PSVs are not darkly stained. A and B, PSVs of a 3-d plant whose tonoplast membranes are strongly labeled (arrows) with anti-α-TIP antibodies (A) but not anti-γ-TIP antibodies (B). Some labeling of vacuolar contents is also seen in A. C and D, Collapsed PSV membranes of 4-d roots label strongly (arrows) with anti-α-TIP antibodies (C) and weakly (arrowheads) with anti-γ-TIP antibodies (D). E and F, In inner cortex cells of 6-d seedlings, virtually all of the α-TIP labeling has disappeared from the newly formed LV membrane (E). In contrast, the γ-TIP labeling of the LV membranes is significantly increased compared with the 4-d samples (F). cVM, Collapsed vacuole membrane. Bars = 200 nm.

such enclosed cytoplasmic domains, the structural organization of the cytoplasm often appeared perturbed when compared with the cytoplasmic regions not surrounded by collapsed tonoplast membranes. The observed changes ranged from an increase/decrease in ribosome density and enhanced ribosome clustering (Fig. 7, B–D) to clear examples of cytoplasmic degradation in autophagosome-like organelles (Fig. 7E; Supplemental Figs. S5 and S6). At more advanced stages of degradation of the remaining contents, the entrapped structures become more lightly stained, and similarly stained material is observed in developing LVs (Figs. 7, C and H). Based on the appearance of these multilamellar compartments exhibiting evidence of cytoplasmic degradation, we postulate that these structures correspond to multilamellar autophagosomes of animal cells (Fengsrud et al., 2000) at different stages of development. In most instances, transformation of these multilamellar autophagic vacuoles into LVs involves engulfment by expansion of the luminal space of the pre-LV domains into outer membrane sheets that surround the autophagic vacuoles (Fig. 7, B, D, E, and H; Supplemental Figs. S6B and S7). However, it is possible that some LVs might fuse directly with autophagic vacuoles (Supplemental Figs. S6 and S8).

DISCUSSION

As reported in this study, seed germination involves not only the mobilization of protein and mineral reserves from PSVs but also the transformation of the reserve-depleted PSVs into LVs. Furthermore, in developing roots, this transformation occurs in a tissue-specific manner, with each cell type exhibiting a unique spatial and/or temporal pattern of differentiation (Fig. 9). The rationale for the cell type specificity of the PSV-dependent LV biogenesis process has yet to be elucidated. It is possible that the simple vacuole transformation process seen in the epidermal and outer cortex cells reflects the fact that once those cells have produced a large LV, their development is largely complete. In contrast, the formation of a large central LV in the inner cortex and vascular bundle cells constitutes only the first of several developmental steps of these cells, and recycling of the amino acids from the cytoplasm via autophagosomes might be needed to support the subsequent stages of cell differentiation.

Cryofixation and Freeze-Substitution Methods Are Important for Preserving the Architecture of Plant Vacuoles for Electron Microscopy Analysis

The hypothesis that PSVs have an ontogenetic relationship to the central vacuole has a long history (Hara and Matsubara, 1980; Van der Wilden et al., 1980; Melroy and Herman, 1991; Olbrich et al., 2007), but the general mechanism of the PSV-to-LV transformation

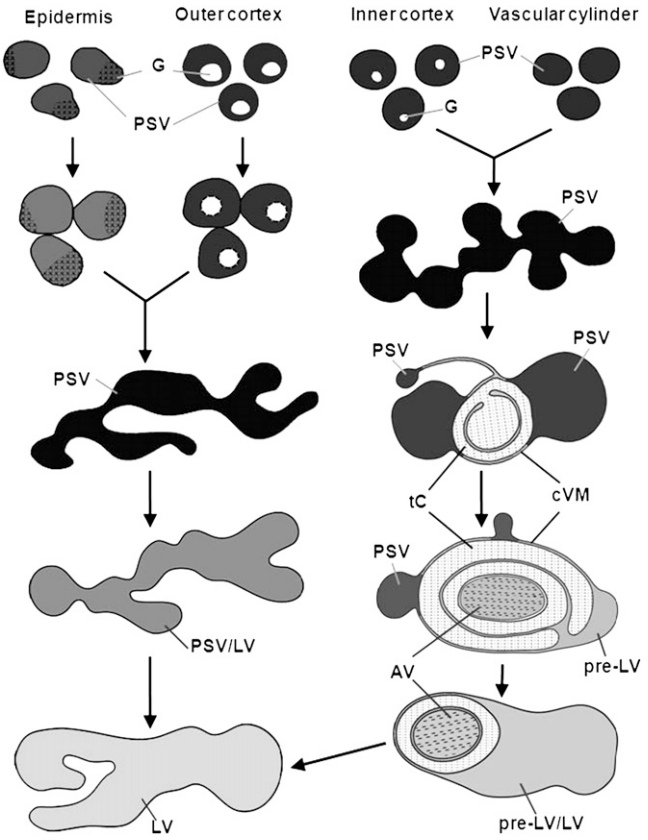

Figure 9. Schematic diagram illustrating the different pathways involved in the transformation of PSVs into LVs in different types of root cells during seed germination and early root development. In epidermal and outer cortex cells, the PSVs fuse together between 2 and 3 DAS to form large vacuoles from which the storage proteins and minerals of the globoids are mobilized. During this mobilization process, the vacuoles are gradually transformed from PSVs into LVs. In epidermal cells, this transformation process is completed by day 4, whereas in the outer cortex cells, the process takes 6 d. A more complex series of conformational changes is involved in the transformation of PSVs to LVs in inner cortex (endodermal) and vascular cylinder cells. Following the fusion of the PSVs into larger PSV-type vacuoles on day 2, the mobilization of the storage molecules during days 3 and 4 induces a gradual osmotic collapse of the vacuolar membranes around the residual PSV contents and the squeezing of these contents into increasingly smaller vacuole domains. The remaining, excess tonoplast membranes simultaneously form collapsed vacuole membrane (cVM) regions, where they become tightly pressed together and produce concentric membrane structures and trapped cytoplasmic (tC) domains. By day 4, some of these concentric double membrane regions begin to form autophagic vacuoles (AV) by encircling cytoplasm and inducing the breakdown of the trapped cytoplasmic materials. In other collapsed membrane domains, a vacuole reinflation process is observed, giving rise to structures called pre-LVs, which during days 5 and 6 gradually expand to form pre-LV/LV transitional-type vacuoles that engulf and digest the autophagic vacuoles. However, we cannot rule out the possibility that the contents of some of the autophagosomes are delivered to the LVs via fusion of the outermost autophagosome membrane with the LV membrane. Upon completion of the autophagic vacuole engulfment fusion and digestion processes (usually on day 6), the formation of the new LVs is complete.

has remained an enigma due to the variability of the electron microscopic images produced during the course of these investigations. As documented here, this variability can be overcome by using cryofixation/freeze substitution instead of chemical fixation/dehydration methods for preserving the samples for electron microscopy analysis. Chemical fixatives such as glutaraldehyde and osmium tetroxide are limited in their ability to preserve transient membrane configurations for structural analysis by the slow rate and selective nature of the chemical cross-linking reactions (Mercy and McCully, 1978; Gilkey and Staehelin, 1986; Samuels et al., 1995; Vos and Hepler, 1998). In addition, chemical fixation cocktails such as zinc-iodine-osmium (Marty, 1978) and osmium ferricyanide (Hepler, 1982), which are used to produce electron-dense deposits within cisternal membrane compartments such as those postulated to give rise to LVs (Marty, 1999), have been shown to cause physical deformation of those membrane compartments (Gilkey and Staehelin, 1986; compare Seguí-Simarro et al., 2004, with Hepler, 1982).

The advantage of high-pressure freezing for preserving cellular structures for structural analysis derives from the fact that during rapid freezing, all cellular molecules (proteins, lipids, sugars, ions, and water) are immobilized simultaneously, in approximately 1 ms (Kiss and Staehelin, 1995). This rate of freezing is fast enough to capture most transient vacuole membrane configurations in their natural state. Furthermore, when this rapid freezing is followed by freeze substitution, all of the water is substituted by acetone at –80°C, which faithfully preserves the three-dimensional architecture of the membranes up to the resin infiltration and polymerization steps. An added bonus is the retention of ions and salts within the vacuoles (Otegui et al., 2002), which we have exploited both to determine the ionic composition of the globoids and of the surrounding PSV matrix (Fig. 2, E–G) and to produce the phytin-dependent black osmium stain of the PSVs in the developing root cells (Figs. 1B, 3, 4, 6, and 7).

The distribution of the darkly staining proteinaceous molecules in the PSVs is also affected by chemical fixation. As documented by Hinz et al. (1995) and by Olbrich et al. (2007), the storage proteins in chemically fixed PSVs and barley (*Hordeum vulgare*) seedlings appear clumped and often aggregated along the deformed inner surface of the vacuole membrane. We observed the same types of darkly stained storage protein aggregates in the PSVs of chemically fixed root tips of tobacco (Supplemental Fig. S10, B, D, and F). This contrasts with the uniform distribution of the darkly stained contents of the PSVs in our high-pressure frozen and freeze-substituted root cells (Figs. 3G, 4G, and 6G; Supplemental Fig. S10, A, C, and E). Based on this result, we postulate that the aggregation of storage proteins in chemically fixed PSVs is a product of the chemical fixation process. This interpretation is also supported by the results of Otegui et al. (2006), who investigated the processing of storage proteins in high-pressure frozen and freeze-substituted Arabidopsis (*Arabidopsis thaliana*) embryos.

In Epidermal and Outer Cortex Cells, the Transformation of PSVs to LVs Is a Mechanically Simple Process Involving PSV Fusion, Reserve Mobilization, and Membrane Restructuring

The simplest mechanism of PSV-to-LV transformation is observed in the meristematic outer cortex (Fig. 3) and epidermal cells (Supplemental Fig. S3) of the radicle. In both of these cell types, dissolution of the globoids and fusion of the swollen PSVs into large vacuoles is completed within 2 to 3 DAS. These vacuoles are initially darkly stained due to the tight binding of osmium to the solubilized phytin molecules. During the following days, the vacuoles increase in size while the osmium staining decreases until no stainable substances can be detected in the vacuole lumen. At this stage of development, the transformed vacuoles become morphologically indistinguishable from LVs (Fig. 3, D and H; Supplemental Fig. S3E). In parallel with these changes in luminal staining, the immunolabeling experiments demonstrated that the α-TIP content of the vacuolar membranes is reduced and the γ-TIP content is increased. This transformation process takes approximately 6 d in the outer cortex cells (Fig. 3D) and approximately 4 d in the epidermal cells (Supplemental Fig. S3E). The biogenesis of LVs in aleurone cells of germinating cereal seedlings (Bethke et al., 1998) closely follows the PSV-to-LV transformation events of epidermal and outer cortical cells in tobacco seedling roots. Thus, in aleurone cells, the transformation events also include coalescence of the PSVs, acidification of the vacuole lumen and enzyme activation, and finally mobilization of the stored molecules. Similar sequences of events have been described for the formation of LVs in germinating seeds of *Prunus serotina* (Swain and Poulton, 1994) and for the generation of large LVs during programmed cell death of endothelial cells in developing Arabidopsis seeds (Ondzighi et al., 2008).

In Inner Cortex (Endodermal) and Vascular Bundle Cells, the PSV-to-LV Transformation Process Involves Complex Changes in Vacuole Architecture as Well as Autophagosome Formation

In contrast to the simple LV-forming events in the epidermal and outer cortex cells, those that accompany the transformation of PSVs to LVs in the inner cortex (endodermis) and vascular cylinder cells are much more complex in that they involve several additional structural intermediates as well as autophagic vacuoles. In both of these latter tissues, the transformation process starts with vacuole fusion at 2 DAS (Figs. 4, A and E, and 6, A and E). By day 3, the first type of novel structure is seen, namely tightly appressed, collapsed vacuole membrane domains linked to the more typical

swollen vacuole domains filled with darkly stained contents (Figs. 4, B, F, and I, and 6, B and F). These collapsed membrane domains, which resemble the collapsed membrane domains of trans-Golgi cisternae (Staehelin et al., 1990; Staehelin and Kang, 2008), appear to be formed by osmotic forces, most likely due to active transport of the solubilized nutrient molecules from the vacuole lumen into the cytoplasm. As in trans-Golgi cisternae, this osmotic collapse causes the luminal materials to be squeezed into the remaining swollen vacuole domains, where the vacuole membrane appears tightly pressed against the vacuole contents (Figs. 4, F and I, 6, G and I, and 7, A and F). Over time, these swollen vacuole domains become smaller (Fig. 7B) and the size of the collapsed membrane domains increases.

The next change involves differentiation of the collapsed membranes into two types of subdomains, one of which forms pre-LVs and the other multilamellar-type autophagosomes/autophagic vacuoles (Fengsrud et al., 2000). We define pre-LVs as reinflated (reswollen) collapsed PSV membranes that exhibit a translucent lumen and label with anti-γ-TIP antibodies (Figs. 4, I and J, 7, B and G, and 8D). Over time, these pre-LV domains are seen to enlarge (Fig. 7D) and to extend into the outer concentric membrane regions that surround the autophagosomes (Fig. 7, E and H). The multilamellar autophagosomes typically form in regions where the collapsed membranes are organized in concentric layers and separated by significant amounts of cytoplasm (Figs. 6, C, G, and I, and 7, A–E and H; Supplemental Fig. S5, A and B). By day 4, many of the trapped cytoplasmic domains begin to show altered morphologies such as increased or decreased numbers of ribosomes (Fig. 7, B–D; Supplemental Figs. S5B and S6, A and B), and at later stages, partially digested membrane fragments are occasionally spotted (Fig. 7E; Supplemental Figs. S6A and S8, A and B). Autophagy is a constitutive process in plant root cells (Yano et al., 2007). A developmental relationship between autophagosome formation and vacuole biogenesis is supported by studies of two Arabidopsis mutants. In the *vacuoleless1* mutant, the biogenesis of LVs in the embryo is blocked and large numbers of autophagosomes accumulate instead (Rojo et al., 2001). Similarly, in the *amsh3* mutant, in which the deubiquitinating enzyme AMSH3 is inactivated, the cells are also incapable of forming large central LVs and also accumulate increased numbers of autophagosomes (Isono et al., 2010).

The final events associated with central LV biogenesis in the inner cortex and vascular bundle cells are the most difficult to interpret due to the multitude of structures seen in our micrographs. Most frequently, we observed what appeared to be an engulfment of the autophagic vacuoles by pre-LV-type vacuolar domains and digestion of the autophagic membranes and their contents (Fig. 7, D, E, and H; Supplemental Figs. S5–S8). However, it is possible that in some instances, the autophagosomes simply fuse with a LV. During this late stage of LV development, the resulting large vacuoles appear filled with flocculent material and small membrane fragments, which disappear over time, yielding the large characteristic LVs of vegetative cells. The engulfment of the multilamellar autophagosomes by the pre-LVs has its parallel in animal cells, where the outermost membrane of multilamellar autophagosomes fuses first with early and late endosomes and subsequently with lysosomes (Liou et al., 1997). A similar set of events has been observed during the engulfment of small vacuoles enriched in overexpressed TIP1-GFP proteins by the central LV in Arabidopsis (Beebo et al., 2009).

It is interesting that some of the vacuole membrane configurations described in this paper have already been reported by others. However, due to the technical limitations associated with specimen preparation discussed above, these earlier researchers were only able to gain glimpses of the transformation events and were unable to develop a coherent hypothesis of LV biogenesis or to show the cell type-specific nature of the transformation events. For example, Buvat (1968) reported on the presence of parallel profiles of smooth ER membranes in meristematic cells of *Hordeum* roots involved in LV formation and postulated that these membranes gave rise to vacuoles via dilations. Most likely, the parallel membranes he described correspond to the concentric, collapsed PSV membranes of this study, but structurally altered by the chemical fixation procedures. However, we have not systematically analyzed the relationship of ER membranes to vacuole membranes during LV biogenesis. Nevertheless, in none of our over 1,000 micrographs have we seen evidence for ER membranes being physically continuous with vacuole membranes.

Amelunxen and Heinze (1984) also provided evidence for an ER origin of LVs in *Linum* seedlings. Their micrographs indicated that the ER tubules line up in a spherical configuration and cause the entrapped cytoplasm to become depleted of ribosomes before the tubules dilate and fuse to form the vacuole. A provacuolar tubular network that stains with zinc-iodide osmium, contains hydrolytic enzymes, and surrounds and entraps cytoplasm before coalescing into LVs forms the basis of the widely cited vacuole biogenesis hypothesis of Marty (1978, 1999). The latter network was postulated to originate from trans-Golgi membranes. Unlike ER membranes, Golgi and trans-Golgi network membranes stain very clearly in high-pressure frozen/freeze-substituted cells and for this reason are easy to recognize in thin section micrographs (Staehelin et al., 1990). In none of our micrographs have we seen evidence suggesting that Golgi or trans-Golgi network cisternae give rise to vacuole-forming long tubular extensions, as postulated by the Marty (1999) hypothesis. We suggest that the spherical, tubular membrane configurations illustrated in the Marty (1978) and Amelunxen and Heinze (1984) studies correspond to LVs with engulfed and partly digested autophagic vacuoles. In such LVs (Supplemental Fig. S8, A and B),

flattened membrane tubules are often seen pressed against the inner surface of the tonoplast membrane, which imparts on them the shape of a central LV. We postulate that the harsh chemical fixation/staining conditions used by the earlier workers led to the fragmentation of the fragile tonoplast membranes, leaving behind the autophagosomal membrane tubules arranged in a central vacuole-like configuration and surrounding the partially degraded contents of the former vacuole lumen (the "partially cleared cytoplasm").

The main contribution of the Olbrich et al. (2007) and the Hunter et al. (2007) vacuole biogenesis studies was the demonstration that all of the developing vacuoles in root cells contain both PSV and LV marker proteins. The importance of these studies lies in the fact that they contradict the predictions of the vacuole biogenesis hypothesis of Paris et al. (1996), which postulates that the large LVs of vegetative cells develop by the merging of separate PSVs and LVs. The immunolabeling results of our investigation are in complete agreement with those of Olbrich et al. (2007), and our ultrastructural results demonstrate that the seedling root cells of tobacco contain only one type of vacuole at any one time of development. Thus, upon rehydration, the radicle cells only contain PSVs, but during subsequent root development, the PSVs are systematically transformed into LVs via cell type-specific pathways.

MATERIALS AND METHODS

Plant Materials and Sample Preparation for Electron Microscopy

Seeds of tobacco (*Nicotiana tabacum*) were surface sterilized, imbibed, and germinated on sterile filter paper moistened by medium containing macronutrients as described by Haughn and Somerville (1986) in vertically positioned petri dishes. Seeds were germinated and grown at room temperature (25°C ± 2°C) in continuous light from 60-W fluorescent lamps. One-millimeter-long segments of root tips of 1- to 6-d-old seedlings were excised while submerged under a 3.5% Suc solution and mounted in high-pressure freezing specimen cups coated with lecithin (Craig and Staehelin, 1988). After freezing, the samples were substituted in 2% OsO_4 in acetone at −80°C for 3 d, warmed to room temperature, and incubated at 40°C for 4 h. After a dry acetone wash at room temperature, samples were infiltrated in Spurr's resin and polymerized at 70°C for 8 h. Thin sections (70 nm thick) were stained with uranyl acetate in 70% methanol for 15 min and lead citrate for 4 min and examined at 80 kV in a Philips CM 10 transmission electron microscope.

For the chemical fixation studies, about 1-mm-long segments of root tips of 1- to 6-d-old seedlings were dissected and fixed (2 h) in 2% (v/v) glutaraldehyde in 25 mmol L^{-1} phosphate buffer (pH 7.2), postfixed (2 h) in 1% (w/v) OsO_4 in 25 mmol L^{-1} phosphate buffer, dehydrated in an acetone series, and infiltrated and embedded in Spurr's resin.

Immunolabeling Experiments

Three-, 4-, and 6-d-old root tips were harvested for high-pressure freezing and freeze substituted in 0.25% glutaraldehyde with 0.1% uranyl acetate in acetone for 3 d at −80°C, washed with acetone at 4°C, and embedded in LR White resin. The LR White sections were incubated first with a milk solution containing 0.1% Tween, then with primary antiserum, followed by the secondary antibody-gold particles (anti-rabbit, 15-nm gold particles). The antibodies used in this study were polyclonal anti-α-TIP and anti-γ-TIP, which were kindly provided by Dr. Maarten Chrispeels (Johnson et al., 1989).

EDXS Analysis

Sections 0.25 to 0.5 μm in thickness were cut with a dry glass knife to avoid washing out the soluble mineral deposits as described by Otegui et al. (2002), mounted on copper grids, flattened onto the grid surface by a very brief exposure to moist air, and then coated with carbon. More than five root tips were used to obtain the EDXS data. The EDXS measurements were carried out on a JEOL JEM-2011 transmission electron microscope equipped with an INCA energy-dispersive spectrometer. Spectra were acquired for 300 s at ×10,000 magnification and an accelerating voltage of 200 kV. Ten spectra of each globoid and its surrounding PSV matrix in this study were obtained. Net counts were obtained by subtracting the background from the peaks.

Measurement of Volume and Surface Area

To analyze the changes in vacuole volume and tonoplast surface area in the root tip meristematic cells, we employed the quantification methods described by Steer (1981). Low-magnification (×4,200) and high-magnification (×12,000) electron micrographs were employed to determine the volume of the cells and vacuoles and the surface area of the tonoplasts, respectively. The low-magnification micrographs were analyzed using a square lattice of lines, 1 cm apart, while for the high-magnification micrographs, an interrupted line grid, based on a square lattice of points with 1-cm spacing, was used. After the total length of the test line was measured and corrected for micrograph magnification, the points and line intersections with the structures of interest, nuclei, vacuoles, nuclear envelope, and tonoplast membranes, were counted. The volume of the cells and vacuoles and the surface area of the tonoplast membranes were then calculated as described by Steer (1981). Micrographs of longitudinal sections of 50 to 150 cells from 10 to 15 different root tips at 1 to 6 DAS were measured. Average volume, surface area, and SD were calculated.

Supplemental Data

The following materials are available in the online version of this article.

Supplemental Figure S1. Longitudinal section of a root tip of a tobacco seedling at 1 DAS.

Supplemental Figure S2. Developmental changes in tobacco root tip anatomy in 2- to 6-d-old seedlings.

Supplemental Figure S3. Electron micrographs of meristematic epidermal cells and their vacuoles at 2, 3, and 4 DAS.

Supplemental Figure S4. Electron micrographs of a meristematic outer cortical cell at 1 DAS.

Supplemental Figure S5. Examples of collapsed vacuole membrane (cVM) structures seen in vascular cylinder cells of 3-, 4-, and 6-d tobacco seedling roots.

Supplemental Figure S6. Example of transitional pre-LV/LV/autophagic vacuole (AV)-type vacuoles in 4-d tobacco seedling root cells.

Supplemental Figure S7. Two examples of pre-LV/LV-type vacuoles in the process of engulfing autophagic vacuoles (AV).

Supplemental Figure S8. Examples of pre-LV/LV vacuoles with engulfed autophagic vacuole-type membrane tubules.

Supplemental Figure S9. Immunogold localization of α-TIP and γ-TIP in the LVs of inner cortex cells in 6-d seedlings.

Supplemental Figure S10. Low and higher magnification micrographs of vacuoles preserved by high-pressure freezing/freeze substitution and chemical fixation in vascular cylinder cells of 4-d tobacco seedling roots.

Supplemental Table S1. Quantitative changes in volume of vascular cylinder, inner cortex, and outer cortex cells and their vacuoles of tobacco root tips from 1- to 6-d-old seedlings.

Received November 29, 2010; accepted January 24, 2011; published January 28, 2011.

LITERATURE CITED

Amelunxen F, Heinze U (1984) On the development of the vacuole in the testa cells of Linum seeds. Eur J Cell Biol **35:** 343–354

Ashton FM (1976) Mobilization of storage proteins of seeds. Annu Rev Plant Physiol **27:** 95–117

Bassham DC (2009) Function and regulation of macroautophagy in plants. Biochim Biophys Acta **1793:** 1397–1403

Beebo A, Thomas D, Der C, Sanchez L, Leborgne-Castel N, Marty F, Schoefs B, Bouhidel K (2009) Life with and without AtTIP1;1, an Arabidopsis aquaporin preferentially localized in the apposing tonoplasts of adjacent vacuoles. Plant Mol Biol **70:** 193–209

Bethke PC, Swanson SJ, Hillmer S, Jones RL (1998) From storage compartment to lytic organelle: the metamorphosis of the aleurone protein storage vacuole. Ann Bot (Lond) **82:** 399–412

Buvat R (1968) Diversite des vacuoles dans les cellules de la racine d'orge (Hordeum sativum) C R Acad Sci Paris **267:** 296–298

Craig S, Staehelin LA (1988) High pressure freezing of intact plant tissue: evaluation and characterization of novel features of the endoplasmic reticulum and associated membrane systems. Eur J Cell Biol **46:** 80–93

De DN (2000) Plant Cell Vacuoles: An Introduction. CSIRO Publishing, Collingwood, Australia

Fengsrud M, Erichsen ES, Berg TO, Raiborg C, Seglen PO (2000) Ultrastructural characterization of the delimiting membranes of isolated autophagosomes and amphisomes by freeze-fracture electron microscopy. Eur J Cell Biol **79:** 871–882

Frigerio L, Hinz G, Robinson DG (2008) Multiple vacuoles in plant cells: rule or exception? Traffic **9:** 1564–1570

Gilkey JC, Staehelin LA (1986) Advances in ultrarapid freezing for the preservation of cellular ultrastructure. J Electron Microsc (Tokyo) **3:** 177–210

Hara I, Matsubara H (1980) Pumpkin (*Cucurbita* sp.) seed globulin. VII. Immunofluorescent study on protein bodies in ungerminated and germinating cotyledon cells. Plant Cell Physiol **21:** 247–254

Haughn GW, Somerville C (1986) Sulfonylurea-resistant mutants of *Arabidopsis thaliana*. Mol Gen Genet **204:** 430–434

He F, Huang F, Wilson KA, Tan-Wilson A (2007) Protein storage vacuole acidification as a control of storage protein mobilization in soybeans. J Exp Bot **58:** 1059–1070

Hepler PK (1982) Endoplasmic reticulum in the formation of the cell plate and plasmodesmata. Protoplasma **111:** 121–133

Herman EM, Larkins BA (1999) Protein storage bodies and vacuoles. Plant Cell **11:** 601–614

Hilling B, Amelunxen F (1985) On the development of the vacuole. II. Further evidence for endoplasmic reticulum origin. Eur J Cell Biol **38:** 195–200

Hinz G, Hoh B, Hohl I, Robinson DG (1995) Stratification of storage proteins in the protein storage vacuole of developing cotyledons of *Pisum sativum* L. J Plant Physiol **145:** 437–442

Höglund AS, Rödin J, Larsson E, Rask L (1992) Distribution of napin and cruciferin in developing rape seed embryos. Plant Physiol **98:** 509–515

Hoh B, Hinz G, Jeong B-K, Robinson DG (1995) Protein storage vacuoles form de novo during pea cotyledon development. J Cell Sci **108:** 299–310

Hunter PR, Craddock CP, Di Benedetto S, Roberts LM, Frigerio L (2007) Fluorescent reporter proteins for the tonoplast and the vacuolar lumen identify a single vacuolar compartment in Arabidopsis cells. Plant Physiol **145:** 1371–1382

Isono E, Katsiarimpa A, Müller IK, Anzenberger F, Stierhof Y-D, Geldner N, Chory J, Schwechheimer C (2010) The deubiquitinating enzyme AMSH3 is required for intracellular trafficking and vacuole biogenesis in *Arabidopsis thaliana*. Plant Cell **22:** 1826–1837

Jauh GY, Phillips TE, Rogers JC (1999) Tonoplast intrinsic protein isoforms as markers for vacuolar functions. Plant Cell **11:** 1867–1882

Jiang L, Phillips TE, Hamm CA, Drozdowicz YM, Rea PA, Maeshima M, Rogers SW, Rogers JC (2001) The protein storage vacuole: a unique compound organelle. J Cell Biol **155:** 991–1002

Johnson KD, Herman EM, Chrispeels MJ (1989) An abundant, highly conserved tonoplast protein in seeds. Plant Physiol **91:** 1006–1013

Kiss JZ, Staehelin LA (1995) High pressure freezing. *In* DM Shotten, ed, Rapid Freezing, Freeze-Fracture and Deep Etching. Wiley-Liss, New York, pp 89–104

Liou W, Geuze HJ, Geelen MJH, Slot JW (1997) The autophagic and endocytic pathways converge at the nascent autophagic vacuoles. J Cell Biol **136:** 61–70

Lott J, Greenwood J, Batten G (1995) Mechanisms and regulation of mineral nutrient storage during seed development. *In* J Kigel, G Galili, eds, Seed Development and Germination. Marcel Dekker, New York, pp 215–235

Marty F (1978) Cytochemical studies on GERL, provacuoles, and vacuoles in root meristematic cells of Euphorbia. Proc Natl Acad Sci USA **75:** 852–856

Marty F (1999) Plant vacuoles. Plant Cell **11:** 587–600

Melroy DL, Herman EM (1991) TIP, an integral membrane protein of the protein-storage vacuoles of the soybean cotyledon undergoes developmentally regulated membrane accumulation and removal. Planta **184:** 113–122

Mercy B, McCully M (1978) Monitoring the course of fixation in plant cells. J Microsc **166:** 43–56

Oda Y, Higaki T, Hasezawa S, Kutsuna N (2009) Chapter 3. New insights into plant vacuolar structure and dynamics. Int Rev Cell Mol Biol **277:** 103–135

Olbrich A, Hillmer S, Hinz G, Oliviusson P, Robinson DG (2007) Newly formed vacuoles in root meristems of barley and pea seedlings have characteristics of both protein storage and lytic vacuoles. Plant Physiol **145:** 1383–1394

Ondzighi CA, Christopher DA, Cho EJ, Chang SC, Staehelin LA (2008) *Arabidopsis* protein disulfide isomerase-5 inhibits cysteine proteases during trafficking to vacuoles before programmed cell death of the endothelium in developing seeds. Plant Cell **20:** 2205–2220

Otegui MS, Capp R, Staehelin LA (2002) Developing seeds of *Arabidopsis* store different minerals in two types of vacuoles and in the endoplasmic reticulum. Plant Cell **14:** 1311–1327

Otegui MS, Herder R, Schulze J, Jung R, Staehelin LA (2006) The proteolytic processing of seed storage proteins in *Arabidopsis* embryo cells starts in the multivesicular bodies. Plant Cell **18:** 2567–2581

Paris N, Stanley CM, Jones RL, Rogers JC (1996) Plant cells contain two functionally distinct vacuoles. Cell **85:** 562–572

Robinson DG, Hinz G (1997) Vacuole biogenesis and protein transport to the plant vacuole: a comparison with the yeast vacuole and the mammalian lysosome. Protoplasma **197:** 1–25

Rojo E, Gillmor CS, Kovaleva V, Somerville CR, Raikhel NV (2001) *VACUOLELESS1* is an essential gene required for vacuole formation and morphogenesis in Arabidopsis. Dev Cell **1:** 303–310

Saito C, Ueda T, Abe H, Wada Y, Kuroiwa T, Hisada A, Furuya M, Nakano A (2002) A complex and mobile structure forms a distinct subregion within the continuous vacuolar membrane in young cotyledons of Arabidopsis. Plant J **29:** 245–255

Samuels AL, Giddings TH Jr, Staehelin LA (1995) Cytokinesis in tobacco BY-2 and root tip cells: a new model of cell plate formation in higher plants. J Cell Biol **130:** 1345–1357

Schlereth A, Standthardt D, Mock HP, Müntz K (2000) Stored cysteine proteinases start globulin mobilization in protein bodies of embryonic axes and cotyledons during vetch (*Vicia sativa* L.) seed germination. Planta **212:** 718–727

Seguí-Simarro JM, Austin JR II, White EA, Staehelin LA (2004) Electron tomographic analysis of somatic cell plate formation in meristematic cells of *Arabidopsis* preserved by high-pressure freezing. Plant Cell **16:** 836–856

Seguí-Simarro JM, Staehelin LA (2006) Cell cycle-dependent changes in Golgi stacks, vacuoles, clathrin-coated vesicles and multivesicular bodies in meristematic cells of *Arabidopsis thaliana*: a quantitative and spatial analysis. Planta **223:** 223–236

Staehelin LA, Giddings TH Jr, Kiss JZ, Sack FD (1990) Macromolecular differentiation of Golgi stacks in root tips of Arabidopsis and Nicotiana seedlings as visualized in high pressure frozen and freeze-substituted samples. Protoplasma **157:** 75–91

Staehelin LA, Kang BH (2008) Nanoscale architecture of endoplasmic reticulum export sites and of Golgi membranes as determined by electron tomography. Plant Physiol **147:** 1454–1468

Steer MW (1981) Quantitative Analysis in Understanding Cell Structure. University of Cambridge Press, Cambridge, UK, pp 24–74

Swain E, Poulton JE (1994) Utilization of amygdalin during seedling development of *Prunus serotina*. Plant Physiol **106:** 437–445

Tiedemann J, Neubohn B, Müntz K (2000) Different functions of vicilin and legumin are reflected in the histopattern of globulin mobilization during germination of vetch (*Vicia sativa* L.). Planta **211:** 1–12

Tiedemann J, Schlereth A, Müntz K (2001) Differential tissue-specific expression of cysteine proteinases forms the basis for the fine-tuned mobilization of storage globulin during and after germination in legume seeds. Planta **212:** 728–738

Van der Wilden W, Herman EM, Chrispeels MJ (1980) Protein bodies of mung bean cotyledons as autophagic organelles. Proc Natl Acad Sci USA **77:** 428–432

Vos JW, Hepler PK (1998) Calmodulin is uniformly distributed during cell division in living stamen hair cells of *Tradescantia virginiana*. Protoplasma **201:** 158–171

Wang J, Li Y, Lo SW, Hillmer S, Sun SSM, Robinson DG, Jiang L (2007) Protein mobilization in germinating mung bean seeds involves vacuolar sorting receptors and multivesicular bodies. Plant Physiol **143:** 1628–1639

Wink M (1993) The plant vacuole: a multifunction compartment. J Exp Bot **44:** 231–246

Xu GX, Tan C, Wei XJ, Gao XY, Zheng HQ (2011) Development of secretory cells and crystal cells in Eichhornia crassipes ramet shoot apex. Protoplasma (in press)

Yano K, Hattori M, Moriyasu Y (2007) A novel type of autophagy occurs together with vacuole genesis in miniprotoplasts prepared from tobacco culture cells. Autophagy **3:** 215–221

Zouhar J, Rojo E (2009) Plant vacuoles: where did they come from and where are they heading? Curr Opin Plant Biol **12:** 677–684